Materials Science Forum Vols. 38-41 (1989) pp 141-150
© (1989) Trans Tech Publications, Switzerland
doi:10.4028/www.scientific.net/MSF.38-41.141

Materials Science Forum Vols. 38-41 (1989) pp. 141-150
Copyright Trans Tech Publications, Switzerland

INTERSTITIAL DEFECT REACTIONS IN SILICON

L.C. Kimerling, M.T. Asom and J.L. Benton(a),
P.J. Drevinsky and C.E. Caefer (b)

(a) AT & T Bell Laboratories
Murray Hill, NJ 07974, USA
(b) Rome Air Development Center
Solid State Sciences Directorate
Hanscom Air Force Base, MA 01731, USA

ABSTRACT. A five level hierarchy of interstitial defect reactions has been observed in silicon involving oxygen, carbon, Group III and Group V impurities. The deep electronic states of the mobile interstitial defects provide a proximity charging effect near a charged reactant which yields a Fermi level dependent reaction cross section. Local structural transformations are observed which exhibit a threshold charge-state behavior. The equilibrium structure of the metastable interstitial iron-acceptor pairs is determined by long range electrostatic, short range elastic and covalency energy terms. Each structural alternative, though compositionally identical, is properly treated as a separate thermodynamic entity.

1. INTRODUCTION

One of the most exciting frontiers in semiconductor materials science has been the discovery of interstitial defect associates, their reactions and structural transformations. Reactions, such as the Watkins replacement mechanism [1], and discussion of structural transformations [2] of the self-interstitial in silicon have been in the literature for over 15 years. However, observation of structural metastability by a variety of capacitance transient measurements and the relation of these phenomena to interstitial defects [3-7] has focused renewed experimental and theoretical attention on the interstitial. Unlike substitutional imperfection, interstitial defects are not confined to host lattice symmetry and often possess multiple atomic configurations with similar total energies. The search for these configurations has led to the detection of a complex hierarchy of defect reactions and an initial glimpse into the relationship between reaction kinetics and structure.

2. REACTIONS OF THE SELF-INTERSTITIAL

One can now account for the reaction sequence of the self-interstitial in both n- and p type silicon. Table I lists the identified defects and their properties. Figure 1 shows the evolution of interstitial defect products with temperature in as many as five stages of reaction. The path

Table I. Interstitial Defect States in Silicon

Defect	E_T eV	Charge State	Stability	REDR	CS	References
$(Si)_iO_i$	-	-	230°K	-	-	8
B_i	E(0.13) E(0.45)	0/+ −/0	240°K	X	X	9,10,11
B_iB_s	H(0.30)	-	>400°C	-	-	12,13
B_iO_i	E(0.26)	-	150-200°C	-	-	12,13
B_iC_s	H(0.29)	-	400°C	-	-	13
C_i	E(012) H(0.27)	−/0 0/+	50°C	X	X	5,18,20,21
C_iC_s	ME(0.17) ME(0.10) MH(0.09) MH(0.05)	−/0 -/0 0/+ 0/+	225°C	X	X	5,14,24
C_iP_s	ME(0.30) ME(0.29) ME(0.23) ME(0.21)	- - -	125°K	X	X	4,5,15,16
C_iO_i	H(0.36)	0/+	400°C	-	-	5,7,15,17,24
Al_i	H(0.23)	+/++	200°C	X	X	18,19

a given reaction sequence will depend on the reactant (background impurity) content of the material. The key to understanding p-type material was a careful series of DLTS studies involving samples of controlled boron, oxygen and carbon content [13]. The breakthrough in understanding n-type material was the detection and assignment of structural metastability for the (C_sC_i) and (P_sC_i) defects, whose DLTS signals are coincident with the dominant vacancy defects, (O_iV) and (P_sV), respectively [5,14]. Some examples from these studies are discussed below.

A. Reaction Hierarchy

A summary of the boron concentration, $[B_s]$, dependence of the introduction rates (by 1 MeV electrons) of room temperature stable defects in p-type silicon is shown in Figure 2. Defect states are identified as E( ), H( ) signifying the electron, hole emission activation energy. ME, MH indicates one of a set of metastable, alternate configurations. In these crucible grown samples, $[O_i] \approx 10^{18}$ cm^{-3}, the vacancy reaction products consist of mainly [VV] and $[O_iV]$ centers. Thus, only interstitial related products are expected to vary with doping level. The initial boron impurity involvement is the production of $[B_i]$ by exchange between (B_s) and $(Si)_i$ [1]. Subsequently, $[B_i]$ migrates throughout the crystal [9] and undergoes *diffusion limited reactions* with background impurities.

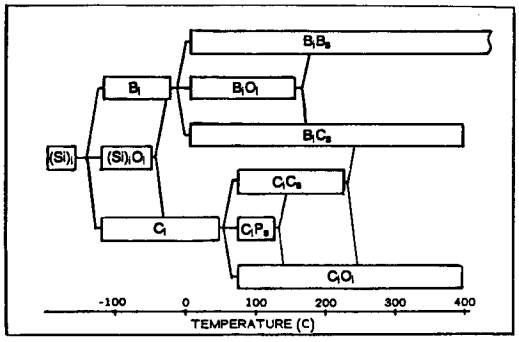

Figure 1. Hierarchy of the self-interstitial defect reactions in silicon. The temperature scale shows the stability of each product under quiescent conditions.

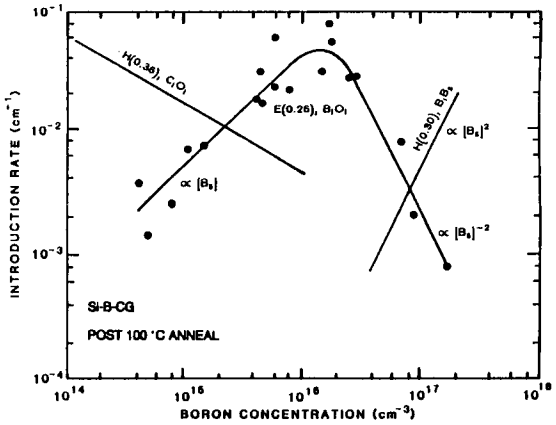

Figure 2. Dependence of interstitial defect introduction rate on the boron content of silicon.

The introduction of E(0.26) increases linearly as a function of $[B_s]$. Supporting data shows a direct dependence on oxygen concentration as well [13]. At high $[B_s]$ the E(0.26) introduction rate decays as $[B_s]^{-2}$. The above results imply that the competing product at high $[B_s]$ is (B_sB_i) whose formation probability is proportional to $\phi \cdot [B_s]^2$ where ϕ is the irradiation fluence. The emergence of H(0.30) with a $[B_s]^2$ dependence fixes its identification as the proposed (B_sB_i) product. The linear dependences of the E(0.26) introduction on both $[B_s]$ and $[O_i]$ led to an assignment of a (B_iO_i) associate [12,13]. At concentrations of $[B_s] > 10^{19}$ cm^{-3}, in n-type material, (B_iB_i) associates are reported to form [22]. The ***disproportionation reaction*** resulting from the negative U character of (B_i) [11]

$$2(B_i)^0 \rightarrow (B_i)^+ + (B_i)^- \qquad (1)$$

may play a role in the attraction of the two identical species.

H(0.36) is not observed in material of low $[O_i]$. Furthermore, its introduction rate decays linearly with increasing $[B_s]$ (Fig. 2) and increases slightly with $[C_s]$ in material of high $[O_i]$. The defect is in direct competition with the production of $[B_iO_i]$. The stability of the defect to 400 °C [12], as shown in Figure 3, provides firm correlation of H(0.36) with (C_iO_i).

Thermal annealing reveals a series of ***dissociation-limited reactions*** among the interstitials and background impurities. Figure 3 shows exemplary isochronal annealing data for the boron-doped samples. All samples behaved similarly with only the distribution of products differing. The fourth level of products emerge at 150 °C when (B_iO_i) reacts to yield (B_iC_s). The temperature at which this reaction occurs increases with $[O_i]$ and ranges between 150 °C for $[O_i] < 8\times10^{15}$ cm^{-3} to 200 °C for $[O_i] = 10^{18}$ cm^{-3}. This shift reflects the influence of the back reaction in the dissociation reaction.

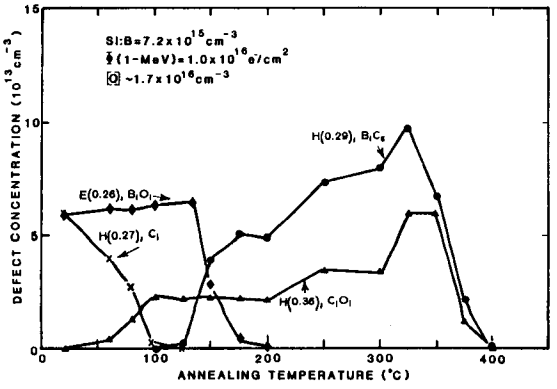

Figure 3. Representative isochronal (20 min) annealing reactions of interstitial defect states in boron-doped silicon.

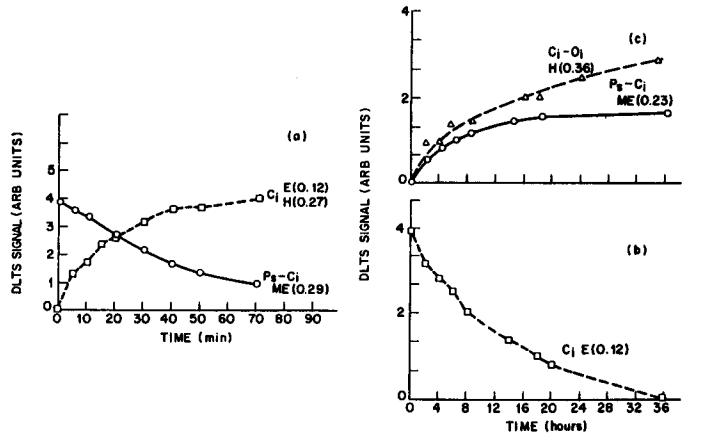

Figure 4. Reversible reactions of C_i with P_sC_i.

$$(B_iO_i) \rightleftarrows (B_i) + (O_i) \quad (2)$$

The H(0.29) product concentration increases in magnitude as $[B_s]$ decreases and is independent of $[O_i]$. At constant $[B_s]$ and $[O_i]$, the fractional conversion of E(0.26) to H(0.29) increases linearly with $[C_s]$. Thus, H(0.29) is assigned to (B_iC_s) which forms as (B_i) is liberated from (B_iO_i).

A second channel of interstitial defect reactions occurs through the (C_i), H(0.27), reactant. (C_s) is a direct competitor with (B_s) for reactions with the self-interstitial, $(Si)_i$ [4]. Besides the (C_iO_i) product discussed above, (C_sC_i) and (P_sC_i) can be formed. These three products control the interstitial reaction pathway in phosphorus-doped silicon [5]. The (P_sC_i) introduction rate increases linearly with phosphorus doping $[P_s]$ [16]. An example of partitioning among these reactions is shown in Figure 4 as (C_i) reacts and as (P_sC_i) dissociates. Key findings revealed in Figure 4 are: 1) the *recombination enhanced defect reaction (REDR)* of the dissociation of (P_sC_i) and diffusion of (C_i); 2) the redistribution of (C_i) among the reaction channels; and 3) the production of one (C_i) for each (P_sC_i) defect removed.

When (C_s) is the dominant background impurity, (C_sC_i) is the favored interstitial product. The production of (B_i) related defects is rapidly quenched as $[C_s]$ increases. The isochronal anneals of Fig. 3 show evidence of (C_i) liberation in the temperature region of dissociation of (C_sC_i), 225 °C, as $[C_iO_i]$ and $[B_iC_s]$ increase. At $T > 400$ °C and/or when the interstitial concentration is greater than that of the impurity reactants, clustering and precipitation of interstitials can occur at a single site [22, 23].

The above results provide new insight into some earlier questions.

1. The (P_sC_i) defect provides the first direct evidence of a Group V-interstitial associate. Modeling of oxidation enhanced diffusion of phosphorus by an interstitial mechanism now has microscopic support.
2. The "two-stage" annealing behavior of E-center defects is actually dissociation of (P_sC_i) at 100 °C and dissociation of (P_sV) at 150 °C. Previous attempts to understand this behavior failed because both defects are produced in proportion to $[P_s]$, both anneal with similar charge-state control and recombination enhancement, and the electrical signals overlap [4]. The true concentration of (P_sC_i) can be determined by transforming it into one of its three metastable configurations.
3. The silicon self-interstitial has a parallel of every known vacancy reaction with the products often more stable.

Table II. Reaction Branching Ratios

Reaction Products	Branching Ratio	Material Type	Reference
$[B_iO_i]/[C_iO_i]$ $\approx [B_i]/[C_i]$	7	p	25
$[B_iB_s]/[B_iO_i]$	12	p	25
$[C_iO_i]/[C_iC_s]$	1,3	n	5,26,27
$[C_iP_s]/[C_iC_s]$	2-12	n	25

B. Reaction Branching Ratios

The ultimate products of $(Si)_i$ reactions are a complex function of the defect and impurity content of the crystal. Table II lists the relative reaction branching ratios, $\frac{k_x}{k_y}$, (when x and y are products), determined by fit of the reactant and product concentrations to

$$[AB] = \frac{k_{AB}[B]}{k_{AB}[B] + k_{AC}[C] + k_{AD}[D]} \tag{3}$$

The above assumes a diffusion limited reaction involving a mobile interstitial defect A with immobile reactants B, C, and D.

Branching ratios near unity reflect similar interaction mechanisms. A geometric reaction cross section yields an interaction distance less than a third neighbor cage radius, $r \leq 5\text{Å}$. The reaction probability is increased when a long range Coulombic interaction ΔH_c is present between oppositely charge species. The capture radius r_c is the distance at which $\Delta H_c = 2$ kT. Thus, $r_c = \frac{Q_A Q_B}{2 \epsilon kT} = 23\text{Å}$ at 300 °K. For the diffusion limited process under consideration $k_{AB} \propto D_A r_{AB}$, where D_A is the diffusion coefficient of (A) and r_{AB} is the capture radius for (A) by (B). A branching ratio of 5-10 indicates competition between long and short range interaction mechanisms. Thus, Table II reveals electrostatically enhanced reactions between $(C_i)^-$ and $(P_s)^+$, $(Si)_i^+$ and $(B_s)^-$, and $(B_i)^+$ and $(B_s)^-$.

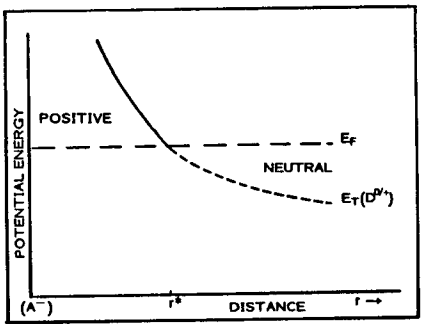

Figure 5. Proximity charging effect of a donor as it approaches a negatively charged acceptor defect.

It is interesting to speculate on why the (P_sC_i) reaction exhibits a range of branching ratios. Two factors are critical to an analysis: 1) The $(C_i)^-$, -/0 acceptor level, E(0.09) is positioned above the Fermi level (at 300 °K) in n-type material doped $n \leq 10^{17}$ cm^{-3}. Thus, (C_i) should be neutral in all experiments reported. 2) (P_sC_i) exhibits 'multistability' with four possible configurations.

A vital link between these two facts and the variable reaction cross section is discussed here as the '*proximity charging effect.*' When two oppositely charged defects approach, their respective defect states are perturbed in energy by the Coulomb interaction such that donor states move toward the conduction band and acceptor states toward the valence band. The ratio of neutral to charged species of a donor approaching a shallow acceptor, for example, is then given by

Table III. Comparison of Relative Site Populations Observed and Calculations for Iron-Acceptor Pairs at 200 °K

	$(Fe_i)^+$				$(Fe_i)^{++}$			
	Measured		Calculated		Measured		Calculated	
Acceptor	N(1)/N(2)	ΔE (eV)	N(1)/N(2)	ΔE (eV)	N(1)/N(2)	ΔE (eV)	N(1)/N(2)	ΔE (eV)
B	$\sim\infty$	>0.1	1.5×10^{10}	.31	$\sim\infty$	>0.1	9.8×10^{14}	0.45
Al	2.2	0.02	2.0	0.02	$\sim\infty$	0.09	580	0.10
Ga	7.0	0.04	3.8×10^{-2}	−0.04	$\sim\infty$	0.14	5.6	0.03
In	0	−0.13	1.5×10^{-5}	−0.16	0.42	0.01	3.7×10^{-4}	−0.12

$$\frac{D^\circ}{D^+} = \exp\left[E_F - \left(E_T(0) + \frac{q_A q_D}{\epsilon r}\right)\right] \tag{4}$$

where E_F is the Fermi level, $E_T(0)$ is the unperturbed energy level of the isolated defect and r is the distance separating the donor D and acceptor A defects.

Simple, shallow impurity levels are pushed out of the gap. Deep level defect states can move into or through the gap, changing charge state with interaction distance. As shown in Fig. 5, a neutral donor acquires a positive charge upon crossing a threshold interaction distance r*. The largest variations in E_T occur at the smallest values of r, and intermediate reaction cross sections result. *Thus, for mobile defects with deep levels, the reaction branching ratio can be a continuous function of the defect energy level and the bulk Fermi level.*

3. BONDING INTERACTIONS

A. Electrostatic and Elastic Energy

The 'proximity charging effect' gives new insight into the mechanism driving local structural transformations for some defects. The iron-acceptor pairs are examples of a relevant system in which the pair structure depends on the charge state of the interstitial iron $(Fe_i)^{0/+/++}$ [28,29,30]. The system exists in two structural states with (Fe_i) located at either the nearest- or second-nearest tetrahedral interstitial position relative to the substitutional acceptor. For (Fe_iB_s), (Fe_iAl_s) and (Fe_iGa_s), the 1st neighbor position is stable and the 2nd neighbor position is metastable. For (Fe_iIn_s) the two structures are bistable, depending on charge state.

In order to understand this behavior we have constructed a simulation of the system including the roles of acceptor size, Coulomb attraction, charge state, and $(Fe)_i$ diffusion [31]. A static silicon lattice of nine unit cells was constructed in three dimensions using the appropriate S_i-S_i interatomic distance of 2.35Å . The (Fe_i)-lattice point interaction was installed as a repulsive potential of the softened Lennard-Jones type: $V(r) = 4E[(\sigma/r)^6]$. For the case of $(Fe_i)^+$, E was scaled so that the saddle point for diffusion matched the measured migration enthalpy, $\Delta H_m = 0.85$ eV [28]. The identity of the acceptor, A, placed on a lattice point was controlled by scaling σ of the repulsive potential at that point by the appropriate radius ratio with respect to silicon.

The charge on the acceptor, Q_A, and interstitial iron donor, Q_{Fe}, sites were included as a simple electrostatic attractive interaction, $V(r) = \frac{Q_{Fe}Q_A}{\epsilon r_{Fe-A}}$. The charge on the (Fe_i) donor was set at 0, +1q or +2q, and the charge on the acceptor was maintained at −1q.

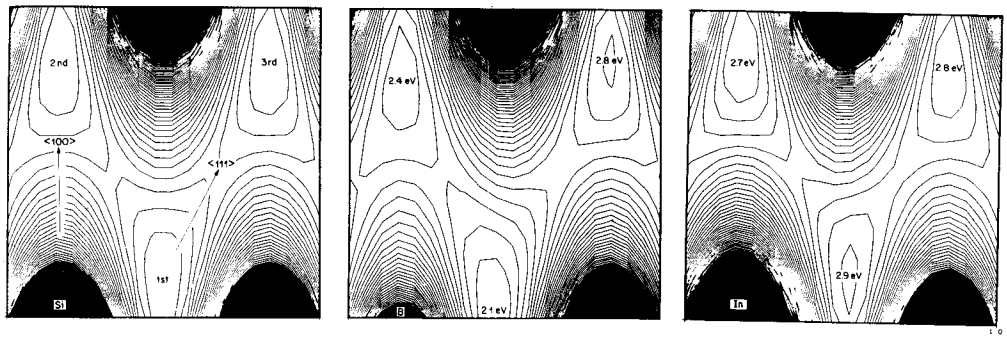

Figure 6. Potential energy contours for $(Fe_i)^+$ in a silicon lattice. (S_i), $(B_s)^-$ and $(In_s)^-$ are placed on the lattice point at the lower left corner of (a), (b) and (c), respectively.

The calculated potential contours associated with $(Fe_i)^+$ diffusion are shown in Fig. 6a. Modifications of these contours by the presence of $(B_s)^-$ or $(In_s)^-$ are shown in Figures 6b and 6c, respectively. The plots show contours of constant potential energy for $(Fe_i)^+$ as a function of its position on a <110> plane in the silicon lattice. Energy minima occur at the first, second and third neighbor tetrahedral interstitial sites relative to the fixed substitutional acceptor. For $(B_s)^-$ the first neighbor site is stable, while for $(In_s)^-$ the second neighbor site is stable. This result explains why (Fe_iB_s) pairs exhibit a trigonal <111> axial symmetry, but (Fe_iIn_s) pairs show a rhombic I, <100> axial symmetry [32].

The competition between the repulsive and attractive forces on a charged (Fe_i) interstitial are graphically displayed in Fig. 7. We trace the potential energy of (Fe_i) for three different charge states as it moves along a <111> back bonding direction from a substitutional $(In_s)^-$ acceptor. The first minimum is the nearest neighbor tetrahedral interstitial site and the second minimum is the third neighbor site. Note that the third neighbor site is lowest in energy for the neutral and +1 charge states, but the first neighbor is lowest for the +2 charge state. This set of configuration diagrams exhibits the classic form of charge state controlled bistability [33]. The phenomenon arises from a competition between repulsive (elastic) and attractive (electrostatic) energy terms. For the case of $(B_s)^-$, no bistability is observed or calculated, because its small size relative to silicon introduces no excess repulsive energy terms.

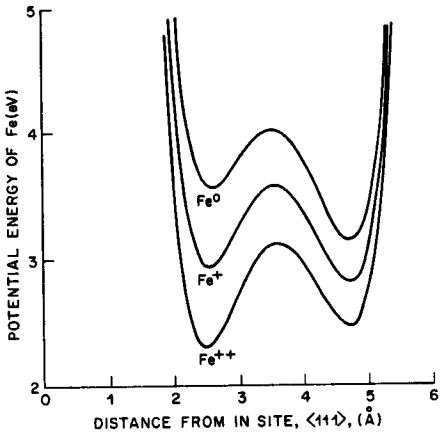

Figure 7. The role of (Fe_i) charge state on the configurational stability of the (Fe_iIn_s) pair.

Table 3 compares the relative populations of the first N(1) and second N(2) neighbor sites, determined by metastability measurements [30], with the results of the static lattice simulation. The difference in total energy at the two sites, ΔE, is also given. The data agree remarkably well with the simulations, although (Fe_iGa) does not follow the expected monotonic trend of increasing

N(2) with increasing acceptor size. For $(Fe_i)^{++}$ the deviations in ΔE for both Ga and In are more pronounced and show an additional stabilization of the first neighbor site by 0.11 eV and 0.13 eV, respectively. (The defect state energy positions for the first neighbor configuration are lowered by similar amounts, showing consistency in both the model and physical behavior of the system.) We propose that this short range stabilization results from bonding covalency supplementing the electrostatic attraction of the pair. The larger acceptor atoms are more polarizable and should show an increasing tendency for a short range component of covalent bonding. Full dynamical simulations are in progress to test this hypothesis.

B. Bond Reconstruction

A unique feature of interstitial defects in semiconductors is their occurrence in both covalently bonded (split, bond centered, delocalized) and ionized, nonbonded (tetrahedral, hexagonal) configurations. The structural configuration is intimately related to the number of bonding electrons, N_{be}, at the defect site. This relationship between defect charge state and structure is the major fundamental challenge in the science of small and intermediate sized systems today.

At one extreme one may employ the octet rule which governs the structure of covalent solids. The predicted equilibrium charge state (CS) is the net excess charge required to yield a filled or empty shell when a summation is made over all atoms, i, of the defect (π bonds also add to the coordination number, CN).

$$\begin{aligned} CS &= \sum_i (N_{be} + CN - 8) \qquad N_{be} \geq 4 \\ &= \sum_i (N_{be} - CN) \qquad N_{be} < 4 \end{aligned} \tag{5}$$

This simple approach predicts that for $N_{be} < 4$, acceptors will have a higher CN configuration than donors, while for $N_{be} \geq 4$, the reverse is expected. In considering electron pair bonds, a charge state change of $\Delta(CS) = \pm 2q$ should require a bond reconstruction, $\Delta(CN)$.

We have examined the charge states of the four-configuration (P_sC_i) defect using TSCAP measurements [33]. The *thermal recovery* sequence of the system from the metastable state by isochronal anneal (following forward bias injection of 10 A/cm^2 at 250 °K) is given below [4].

$$ME(0.2) \xrightarrow{Ob} ME(0.29) \underset{V_R}{\overset{Ob}{\rightleftarrows}} ME(0.23) \xrightarrow{Ob} ME(0.30) \tag{6}$$

The reverse process of *injection stimulated transformation* at 250 °K using lower current densities of 10^{-3}-10^{-2} A/cm^2 shows the reverse sequence

$$ME(0.30) \rightarrow ME(0.23) \rightarrow ME(0.29) \rightarrow ME(0.21) \tag{7}$$

with some C_i, E(0.12), being emitted. The mirror symmetry between the injection stimulated sequence and the thermally stimulated approach to equilibrium suggests that the ordering ME(0.21) → ME(0.30) is fundamental. Measurement of the total system charge in each state by TSCAP shows that ME(0.30) and ME(0.23) possess a charge state which is −2q more negative than ME(0.29). We assume for simplicity that the former are acceptors and the latter is a donor. Thus, the charge state controlled transformation $ME(0.29) \underset{V_R}{\overset{Ob}{\rightleftarrows}} ME(0.23)$ is a likely candidate for bond reconstruction, and this complex system may simplify to two sets of configurations separated by a bond reconstruction reaction.

A simple example of bond reconstruction is the *interstitial handoff* process observed in p-type silicon. The isochronal annealing curve of Fig. 3 shows an increase in the concentrations of the (C_iO_i) and (B_iC_s) defects at 225 °C. This reaction is fed by the dissociation of (C_sC_i) which occurs at this temperature. Thus, C_i is transformed into B_i by the reaction.

$$(C_i) + (B_s) \rightarrow (B_iC_s) \quad (8)$$

This handoff procedure is equivalent to the Watkins replacement mechanism for the self-interstitial. Both reactions are of the bond reconstruction type.

4. SUMMARY

Interstitial defect reactions in semiconductors provide fundamental insight into the relationship between structure and function in chemistry. Interstitial defects are very reactive and yield products involving species across the Periodic Table. Recombination enhanced motion, metastability, proximity charging, and site exchange are among the phenomena observed. The reactions involve both long and short range atomic motion. The high mobility of interstitials yields an abundance of reactions and reaction mechanisms. The multi-configurational freedom available to interstitial defects makes each system complex in its analysis but rich in new phenomena.

REFERENCES

[1] Watkins, G.D.: in Radiation Damage in Semiconductors (Dunod, Paris, 1965), p. 97
[2] Seeger, A., and Frank, W., in Radiation Damage and Defects in Semiconductors, ed. by Whitehouse, J.E. (Inst. Phys. Conf. Ser. 19, London, 1973) p. 262.
[3] Levinson, M., Benton, J.L., and Kimerling, L.C.: Phys. Rev., 1983, B27, 6216
[4] Chantre, A. and Kimerling, L.C.: Appl. Phys. Lett., 1986, 48, 1000
[5] Asom, M.T., Benton, J.L., Sauer, R. and Kimerling, L.C.: Appl. Phys. Lett., 1987, 51, 256
[6] Song, L.W., Benson, B.W. and Watkins, G.D.: Appl. Phys. Lett., 1987, 51, 1155
[7] Trombetta, J.M., and Watkins, G.D.: Appl. Phys. Lett., 1987, 51, 1103
[8] Brelot, A., and Charlemagne, J.: Rad. Effects, 1971, 8, 61
[9] Watkins, G.D.: Phys. Rev., 1975, B12, 5824
[10] Troxell, J.R., and Watkins, G.D., Phys. Rev., 1980, B22, 921
[11] Harris, R.D., Newton, J.L., and Watkins, G.D.: Phys. Rev. Lett., 1982, 48, 1271
[12] Drevinsky, P.J., and DeAngelis, H.M.: in Thirteenth International Conference on Defects in Semiconductors, ed. by Kimerling, L.C., and Parsey, Jr., J.M., (The Metallurgical Society of AIME, Warrendale, PA, 1985), p. 807.
[13] Drevinsky, P.J., Caefer, C.E., Tobin, S.P., Mikkelsen, Jr., J.C., and Kimerling, L.C.: in Defects in Electronic Materials, ed. by Stavola, M., Pearton, S.J., and Davies, G., (Mater. Res. Soc. Proc. 104, Pittsburgh, 1988), p. 167.
[14] Song, L.W., Zhan, X.D., Benson, B.W., and Watkins, G.D.: Ibid., p. 79
[15] Benton, J.L., Asom, M.T., Sauer, R., and Kimerling, L.C.: Ibid., p. 85
[16] Chantre, A.M., Asom, M.T., Benton, J.L., and Kimerling, L.C.: Mater. Sci. Forum, 1986, 10-12, 163.
[17] Newman, R.C., and Bean, A.R.: Rad. Effects, 1971, 8 189
[18] Kimerling, L.C.: in Radiation Effects in Semiconductors 1976, ed. by Urli, N.B. and Corbett, J.W. (Inst. Phys. Conf. Ser. 31, London, 1977), p. 221
[19] Troxell, J.R., Chattergee, A.P., Watkins, G.D., and Kimerling, L.C.: Phys. Rev., 1979, B19, 5336
[20] Kimerling, L.C., Blood, P.W., and Gibson, W.M.: in Defects and Radiation Effects in Semiconductors 1978, ed. by Albany, H.J., (Inst. Phys. Conf. Ser. 46, London, 1979), p. 273
[21] Harris, R.D., and Watkins, G.D.: in Thirteenth International Conference on Defects in Semiconductors, ed. by Kimerling, L.C., and Parsey, Jr., J.M., (The Metallurgical Society of AIME, Warrendale, PA, 1985), p. 799
[22] Tipping, A.K. and Newman, R.C.: Semicond. Sci. Technol., 1987, 2, 389
[23] Chappell, S.P. and Newman, R.C.: Semicond. Sci. Technol., 1987, 2, 691

[24] Murin, L.I.: Phys. Stat. Sol., 1986, a93, K147
[25] Drevinsky, P.J., Benton, J.L., and Kimerling, L.C.: to be published.
[26] Akhmetov, V.D., and Bolotov, V.V.: Phys. Stat. Sol., 1982, a72, 61
[27] Davies, G., Lightowlers, E.C., Newman, R.C., and Oates, A.S.: Semicond. Sci. Technol. 1987, 2, 524
[28] Kimerling, L.C. and Benton,J.L.: Physica, 1983, 116B, 297
[29] Chantre, A. and Bois, D.: Phys. Rev., 1985, B31, 7979
[30] Chantre, A. and Kimerling, L.C.: Mater. Sci. Forum, 1986, 10-12, 387
[31] Kimerling, L.C., Benton, J.L. and Gilmer, G.H.: to be published
[32] Ludwig, G.W. and Woodbury, H.H.: in Solid State Physics, ed. by Ehrenreich, H., Seitz, F., and Turnbull, D. (Academic Press, New York, 1962), vol. 13, p. 223
[33] Benton, J.L. and Levinson, M.: in Defects in Semiconductors II, ed. by Mahajan, S. and Corbett, J.W. (Mat. Res. Soc. Proc. 14, New York, 1983), p. 95
[34] Kimerling, L.C. and Benton, J.L.: to be published

Defects in Semiconductors 15
10.4028/www.scientific.net/MSF.38-41

Interstitial Defect Reactions in Silicon
10.4028/www.scientific.net/MSF.38-41.141